

Optical pulsations from the anomalous X-ray pulsar 1E 1048.1–5937

V. S. Dhillon,^{1*} T. R. Marsh,² S. P. Littlefair,¹ C. M. Copperwheat,² P. Kerry,¹
R. Dib,³ M. Durant,⁴ V. M. Kaspi,³ R. P. Mignani,⁵ A. Shearer⁶

¹*Department of Physics and Astronomy, University of Sheffield, Sheffield S3 7RH, UK*

²*Department of Physics, University of Warwick, Coventry CV4 7AL, UK*

³*Department of Physics, McGill University, Montreal, Quebec H3A 2T8, Canada*

⁴*Instituto de Astrofísica de Canarias, 38200 La Laguna, Tenerife, Spain*

⁵*Mullard Space Science Laboratory, University College London, Holmbury St. Mary, Dorking, Surrey, RH5 6NT, UK*

⁶*Centre for Astronomy, National University of Ireland, Galway, Newcastle Rd., Galway, Ireland*

Submitted on 2008 November 12.

ABSTRACT

We present high-speed optical photometry of the anomalous X-ray pulsar 1E 1048.1–5937 obtained with ULTRACAM on the 8.2-m Very Large Telescope in June 2007. We detect 1E 1048.1–5937 at a magnitude of $i' = 25.3 \pm 0.2$, consistent with the values found by Wang et al. (2008) and hence confirming their conclusion that the source was approximately 1 mag brighter than in 2003–2006 due to an on-going X-ray flare that started in March 2007. The increased source brightness enabled us to detect optical pulsations with an identical period (6.458 s) to the X-ray pulsations. The rms pulsed fraction in our data is $21 \pm 7\%$, approximately the same as the 2–10 keV X-ray rms pulsed fraction. The optical and X-ray pulse profiles show similar morphologies and appear to be approximately in phase with each other, the latter lagging the former by only 0.06 ± 0.02 cycles. The optical pulsations in 1E 1048.1–5937 are very similar in nature to those observed in 4U 0142+61. The implications of our observations for models of anomalous X-ray pulsars are discussed.

Key words: pulsars: individual: 1E 1048.1–5937 – stars: neutron

1 INTRODUCTION

The anomalous X-ray pulsars (AXPs) are a small group¹ of isolated neutron stars in which the X-ray luminosity far exceeds the energy available from the spin-down. The AXPs are generally believed to be magnetars, in which the excess luminosity is powered by the decay of an ultra-strong magnetic field, in excess of 10^{14} G (see Woods & Thompson 2006). An alternative explanation is the fallback disc scenario, in which some of the supernova ejecta fails to escape and forms an accretion disc around the neutron star, providing an extra source of energy to power the X-ray emission (van Paradijs et al. 1995; Chatterjee et al. 2000; Alpar 2001).

One way of discriminating between the magnetar and

fallback disc models is via optical observations. The magnetar model predicts any optical emission must be non-thermal and magnetospheric in origin. Four plausible mechanisms have been considered – coherent plasma emission, synchrotron emission from electrons with high Lorentz factors, cyclotron emission from ions in the outer magnetosphere and curvature emission from bunched electron-positron pairs in the inner magnetosphere (see Beloborodov & Thompson (2007) and references therein). The fallback disc model, on the other hand, predicts any optical emission is produced by reprocessing of the X-ray light in the disc and/or thermal emission from the disc (Perna et al. 2000).

The first AXP to be detected in the optical part of the spectrum was 4U 0142+61 (Hulleman et al. 2000). Optical pulsations were discovered in 4U 0142+61 by Kern & Martin (2002), and the fact that these pulsations have the same period, morphology and phase as the X-rays, but with 5–7 times greater pulsed fraction, was reported by Dhillon et al. (2005). These results provided strong support for the magnetar model – pulsed optical emission is indicative of a mag-

* E-mail: vik.dhillon@sheffield.ac.uk

¹ See <http://www.physics.mcgill.ca/~pulsar/magnetar/main.html> for an up-to-date catalogue of all known AXPs, including the various wavelengths at which each has been detected.

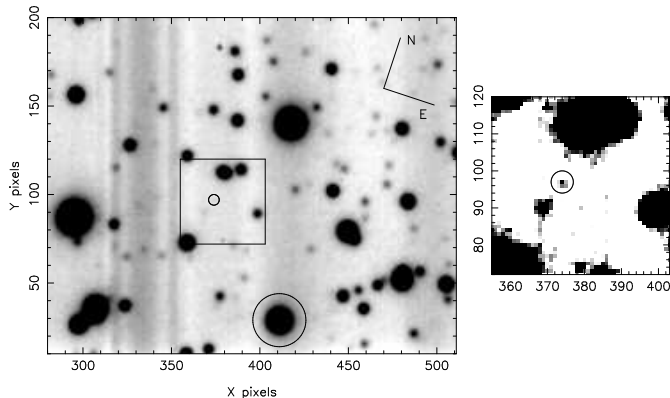


Figure 1. Left: Summed i' -band image of the field around 1E 1048.1–5937, with a total exposure time of 10 684 s. For clarity, only a portion of one of the two ULTRACAM windows is shown. The positions of 1E 1048.1–5937 and the comparison star are indicated by circles near the centre and bottom of the image, respectively. The central box shows the portion of the field that is plotted at a higher contrast on the right. The orientation of the image is marked on the upper right-hand side. The pixel scale is 0.156 arcseconds/pixel, hence the field of view in this image is 36×30 arcseconds. The vertical banding is due to residual bias structure. Right: Higher contrast plot of a 7.5×7.5 arcsecond field around 1E 1048.1–5937, highlighting the detection of the pulsar in the i' -band

netospheric origin and disc reprocessing is unlikely in this case, as the optical pulsed fraction is higher than the X-ray pulsed fraction and there is no time delay between the two. Although it is possible to contrive ways in which the fallback disc model is consistent with the optical pulsations observed in 4U 0142+61, e.g. by assuming that the X-ray pulse profile that we observe is different to the X-ray radiation seen by the disc due to orientation or beaming effects, or by invoking a hybrid disc-magnetosphere model (see Ertan et al. (2007) and references therein), the weight of evidence from the optical and other wavelengths lies heavily on the side of the magnetar model (see Mereghetti (2008) for a recent review).

The detection of optical pulsations in other AXPs would provide valuable confirmation, or otherwise, of the results for 4U 0142+61 discussed above. Only one other AXP has been unambiguously identified in the optical: 1E 1048.1–5937 (Durant & van Kerkwijk 2005)¹. In this paper we report on the first detection of optical pulsations from AXP 1E 1048.1–5937, obtained only ~ 3 months after a bright X-ray flare in March 2007.

2 OBSERVATIONS AND DATA REDUCTION

The observations of 1E 1048.1–5937 presented in this paper were obtained with ULTRACAM (Dhillon et al. 2007) at the Nasmyth focus of Melipal, the 8.2-m Unit 3 of the Very Large Telescope (VLT) in Chile. ULTRACAM is a CCD camera designed to provide imaging photometry at high temporal resolution in three different colours simultaneously. The instrument provides a 2.66 arcminute field on its three 1024×1024 E2V 47-20 CCDs (i.e. 0.156 arcseconds/pixel). Incident light is first collimated and then split into three different beams using a pair of dichroic beamsplit-

Table 1. X-ray ephemeris for 1E 1048.1–5937 (Dib et al. 2008). The epoch of the frequency and frequency derivative measurements given below falls on the same night as our VLT observations (09/06/2007 = MJD 54 260). BMJD refers to the Barycentric-corrected Modified Julian Date on the Barycentric Dynamical Timescale (TDB). The errors on the last two digits of each parameter are given in parentheses. This ephemeris is valid for BMJD 54 229.0 – 54 280.0.

ν (Hz)	0.1548479469(42)
$\dot{\nu}$ (10^{-13} Hz s $^{-1}$)	–5.413(53)
Epoch (BMJD)	54 260.0

ters. For the observations presented here, one beam was dedicated to the SDSS u' ($\lambda_{eff} = 3543\text{\AA}$) filter, another to the SDSS g' (4770\AA) filter and the third to the SDSS (7625\AA) i' filter. Because ULTRACAM employs frame-transfer chips, the dead-time between exposures is negligible: we used ULTRACAM in its two-windowed mode, each of 250×200 pixels, resulting in an exposure time of 0.963 s and a dead-time of 0.024 s. A total of 11 095 frames of 1E 1048.1–5937 were obtained on the night of 2007 June 9, with each frame time-stamped to a relative (i.e. frame-to-frame) accuracy of $\sim 50 \mu\text{s}$ and to an absolute accuracy of ~ 1 ms using a dedicated GPS system (see Dhillon et al. 2007). Observations of the SDSS standard G163-51 (Smith et al. 2002) were also obtained to flux calibrate the data. The night was photometric, with no moon and i' -band seeing of 0.65 arcseconds. The sum of the 11 095 frames in the i' -band is shown in figure 1, which can be compared to the finding charts presented by Durant & van Kerkwijk (2005).

The data were reduced using the ULTRACAM pipeline software (Dhillon et al. 2007). All frames were first debiased and then flat-fielded, the latter using the median of twilight sky frames taken with the telescope spiralling. Adopting the same successful approach that we used in our study of AXP 4U 0142+61 (Dhillon et al. 2005), we extracted light curves of 1E 1048.1–5937 using two different techniques:

2.1 Technique (i)

As part of a long-term monitoring project, 1E 1048.1–5937 has been observed regularly (up to three times per week) since 1997 with the Proportional Counter Array (PCA) on board the Rossi X-ray Timing Explorer (RXTE) [Kaspi et al. 2001; Gavriil & Kaspi 2004; Dib et al. 2008]. The X-ray spin frequency and frequency derivative of 1E 1048.1–5937 for the night of our VLT observations (MJD 54 260) are given in table 1. For the first light-curve extraction technique, we shifted and added each of the 11 095 ULTRACAM frames into 10 evenly-spaced phase bins using the epoch and spin frequency given in table 1, resulting in 10 high signal-to-noise data frames. An optimal photometry algorithm (Naylor 1998) was then used to extract the counts from 1E 1048.1–5937 and an $i' \sim 17$ comparison star ~ 12 arcseconds to the south-east of the AXP (see figure 1), the latter acting as the reference for the profile fits and transparency-variation correction. The position of 1E 1048.1–5937 relative to the comparison star was deter-

mined from a sum of all the images, and this offset was then held fixed during the reduction so as to avoid aperture centroiding problems. The sky level was determined from a clipped mean of the counts in an annulus surrounding the target stars and subtracted from the object counts.

2.2 Technique (ii)

The second approach we took to light curve extraction was identical to that described above, except we omitted the phase-binning step and simply performed optimal photometry on the 11 095 individual ULTRACAM data frames followed by a periodogram analysis of the resulting time series. In other words, we made no assumption about the spin period of 1E 1048.1–5937.

3 RESULTS

3.1 Magnitudes

We were unable to detect 1E 1048.1–5937 in u' and g' , at a 3σ detection limit of $u' > 25.7$ and $g' > 27.6$, respectively. This is unsurprising given the high visual extinction to the object ($A_V = 4.9$; Durant & van Kerkwijk 2006). We did, however, clearly detect 1E 1048.1–5937 in i' at a magnitude of $i' = 25.3 \pm 0.2$, as shown in figure 1. Durant & van Kerkwijk (2005) found that 1E 1048.1–5937 was at a magnitude of $I = 26.2 \pm 0.4$ ($i' \sim 26.1$)² on 06/06/2003, just over one year after its first X-ray flare was observed in April 2002. Wang et al. (2008) observed 1E 1048.1–5937 at a magnitude of $I = 24.9 \pm 0.2$ ($i' \sim 24.8$)² on 07/05/2007, just over one month after its second X-ray flare began on 2007 March 21. These authors also measured a limit of $i' > 24.5$ on 15/07/2007. Our i' -band magnitude, which is slightly fainter and was obtained slightly later than the first I -band measurement of Wang et al. (2008), implies that we observed 1E 1048.1–5937 whilst it was still relatively bright, but declining, from the most recent X-ray flare (see Tam et al. 2008).

3.2 Pulse profiles

The two data reduction techniques described in section 2 result in two different pulse profiles for 1E 1048.1–5937.

3.2.1 Technique (i)

The first technique produced the pulse profile shown by the solid line in the top panel of figure 2. The pulse profile exhibits a broad, single-humped structure with a peak around phase 0.5 and a minimum around phase 0. There is a great deal of similarity in the morphologies of the optical pulse profile shown in the top panel of figure 2 and the 2–10 keV X-ray pulse profile shown below it, where the

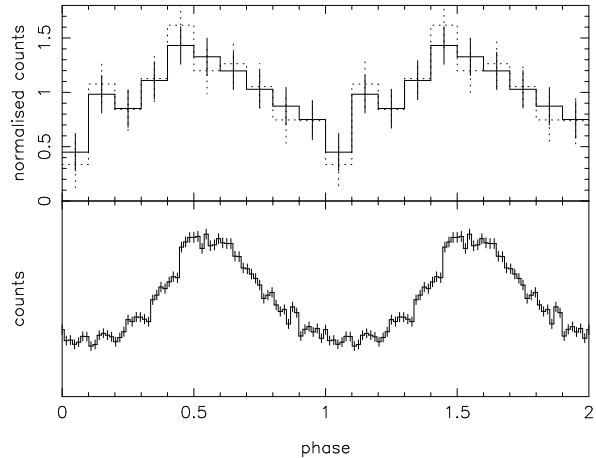


Figure 2. Top: The solid and dotted lines show optical pulse profiles of 1E 1048.1–5937 in the i' -band obtained using techniques (i) and (ii), respectively (see sections 2.1 and 2.2). Each pulse profile was first corrected for transparency variations using the comparison star shown in figure 1, although the correction made only a negligible difference to the light curves. The pulse profiles were then normalised by dividing by the mean number of counts. For clarity, two cycles are shown. Bottom: Averaged X-ray pulse profile of 1E 1048.1–5937 in the 2–10 keV energy band spanning the epoch of the optical observations (Dib et al. 2008). Note that it is not possible to estimate the X-ray pulsed fraction from this profile as the PCA on RXTE has a 1° field of view and no imaging capability, rendering the background level uncertain. For this reason, no scale is given on the ordinate.

latter is the average of the X-ray light curves in the period 23/05/2007–21/06/2007 obtained as part of the RXTE monitoring campaign described by Dib et al. (2008), with a total effective integration time of 59.5 ks. Both profiles show the same broad, single-humped morphology. Moreover, since the X-ray light curve shown in figure 2 has also been phased using the ephemeris given in table 1, it can be seen that the optical and X-ray pulse profiles are approximately in phase with each other. To quantify this, the optical pulse profile was cross-correlated with the X-ray pulse profile. The resulting peak in the cross-correlation function was fitted with a Gaussian to derive a phase shift of -0.06 ± 0.02 cycles (i.e. -0.39 ± 0.13 s), where a negative phase shift implies that the X-ray pulse profile lags the optical pulse profile. This phase shift is only significant at the 3σ level, due to the low signal-to-noise and time resolution of the optical data, and additional data will be required in order to confirm that the phase shift is different from zero (discounting the unlikely situation in which the time delay is approximately equal to some multiple of the spin period).

It should be noted that the morphology of the X-ray pulse profile in 1E 1048.1–5937 does not appear to be energy sensitive; the shapes of the 2–4 keV and 6–10 keV pulse profiles are virtually identical to the 2–10 keV pulse profile shown in figure 2, even though the 6–10 keV band is composed primarily of non-thermal photons whereas the 2–4 keV band is composed of both thermal and non-thermal photons (F. Gavriil, private communication).

The modulation amplitude of the pulses presented in figure 2 can be measured using a peak-to-trough pulsed fraction, h_{pt} , defined as follows:

² Noting that the visual extinctions to 1E 1048.1–5937 and 4U 0142+61 are approximately the same (Durant & van Kerkwijk 2006), we have assumed that the colours of 1E 1048.1–5937 are the same as 4U 0142+61 (Hulleman et al. 2004; Dhillon et al. 2005) and then used the equations of Smith et al. (2002) to convert from I to i' .

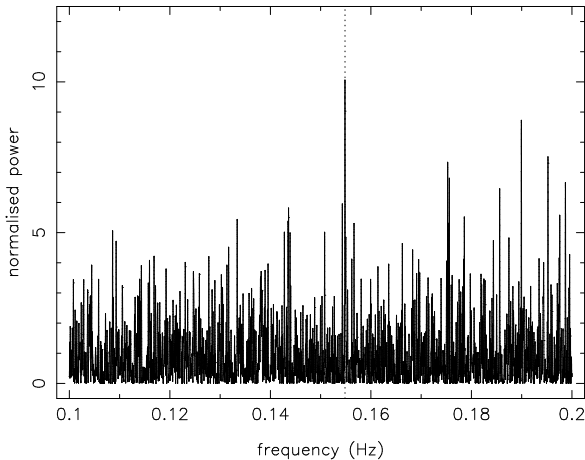


Figure 3. Lomb-Scargle periodograms of 1E 1048.1–5937 in the i' -band, obtained using the light curves from technique (ii) [section 2.2]. The dotted line shows the X-ray pulse frequency of 0.1548479469 Hz given in table 1.

$$h_{pt} = \frac{F_{max} - F_{min}}{F_{max} + F_{min}}, \quad (1)$$

where F_{max} and F_{min} are the maximum and minimum flux in the pulse profile, respectively. We find a value of $h_{pt} = 52 \pm 15\%$. The peak-to-trough pulsed fraction defined in equation 1 effectively adds any noise present in the light curve to the true pulsed fraction, thereby tending to increase the resulting measurement. A more robust estimate is given by the root-mean-square (rms) pulsed fraction, h_{rms} , defined as follows:

$$h_{rms} = \frac{1}{\bar{y}} \left[\frac{1}{n} \sum_{i=1}^n (y_i - \bar{y})^2 - \sigma_i^2 \right]^{\frac{1}{2}}, \quad (2)$$

where n is the number of phase bins per cycle, y_i is the number of counts in the i^{th} phase bin, σ_i is the error on y_i and \bar{y} is the mean number of counts in the cycle. As expected, measuring the optical pulsed fraction in this way gives a lower value of $h_{rms} = 21 \pm 7\%$.

For comparison, the 2–10 keV X-ray rms pulsed fraction at the same epoch as the optical observations was $h_{rms} = 28.7 \pm 0.5\%$. Since it isn't possible to measure the rms pulsed fraction directly from the RXTE pulse profile due to the uncertain background (see caption to figure 2), we derived this value as follows. We first averaged the rms pulsed fraction, defined as the product of the total flux and the rms pulsed fraction, measured with RXTE between 2007 June 7 and June 12 (Dib et al. 2008). This value, which is background independent, was identical to that measured with *Chandra* on 2007 April 28 by Tam et al. (2008), who also find a strong anticorrelation between total flux and rms pulsed fraction. Hence if the pulsed flux was the same for the RXTE and *Chandra* observations, we can be confident that the rms pulsed fraction was the same as well, and hence we have adopted the *Chandra* rms pulsed fraction from the 2007 April 28 observation of Tam et al. (2008).

3.2.2 Technique (ii)

The second data reduction technique (section 2.2) can be used to provide a check on the reliability of the optical pulse

profile derived using technique (i). Rather than adopting the X-ray ephemeris given in table 1, we can instead determine the pulse period directly from our optical data using a periodogram. Measuring the same period in the optical and the X-rays would prove without doubt that we have detected optical pulsations from 1E 1048.1–5937.

Figure 3 shows the Lomb-Scargle periodograms (Press & Rybicki 1989) for the 11 095 points in the i' -band light curves. The light curve was first corrected for transparency variations. The highest peak in the resulting periodogram occurs at a frequency of 0.15484 ± 0.00004 Hz (6.458 ± 0.002 s), where the error is given by the width (σ) of a Gaussian fit to the peak in the periodogram. This frequency is consistent to the fifth decimal place with the X-ray pulse frequency given in table 1, thereby confirming that we have indeed detected the X-ray pulsation of 1E 1048.1–5937 in the optical. We further tested the robustness of our period detection by constructing 10 000 randomised light curves from the original light curves by randomly re-ordering the time-series. None of the resulting 10 000 periodograms showed a higher peak at 0.15484 Hz. To check for artifacts, we calculated the Lomb-Scargle periodograms of both the sky and the comparison star – neither showed any evidence for a periodicity at 0.15484 Hz, or at any other frequency. We also searched for evidence of optical bursts and/or longer-timescale periodicities in our 10 684 s light curve – nothing significant was found.

Folding the 11 095 points of the technique (ii) light curve on the X-ray period given in table 1 results in the pulse profile shown by the dotted line in the top panel of figure 2. Note that the phasing of both the technique (i) and (ii) profiles in figure 2 can be directly compared, as all data have been folded using the zero point given in table 1. As one would expect, the technique (ii) light curve shown is in excellent agreement in terms of morphology, phasing and pulsed fraction ($h_{rms} = 26 \pm 8\%$) with the technique (i) light curve, lending additional confidence to our reduction and analysis techniques.

4 DISCUSSION AND CONCLUSIONS

The results presented in section 3 demonstrate conclusively that we have detected optical pulsations from 1E 1048.1–5937 on the X-ray spin period.

It is instructive to compare the optical light curve of 1E 1048.1–5937 with that of the only other AXP to have been studied in this way – 4U 0142+61 (Dhillon et al. 2005). Both objects show optical pulsations on the X-ray spin period, which is 6.458 s in the case of 1E 1048.1–5937 and 8.688 s in 4U 0142+61. Both objects show optical pulsations with similar morphologies to their 2–10 keV X-ray light curves, with 1E 1048.1–5937 exhibiting a single-humped pulsation and 4U 0142+61 a double-humped pulsation. Both objects exhibit optical pulsations which are approximately in phase with the X-ray pulsations, with 1E 1048.1–5937 showing only marginal evidence for the optical leading the X-rays and 4U 0142+61 showing only marginal evidence for the optical lagging the X-rays. Even the optical pulsed fractions of the two objects are similar, with values of $h_{pt} = 52 \pm 15\%$ and $h_{rms} = 21 \pm 7\%$ in 1E 1048.1–5937, and $h_{pt} = 58 \pm 16\%$ and $h_{rms} = 29 \pm 8\%$ in 4U 0142+61.

The only major difference when comparing this study of 1E 1048.1–5937 with Dhillon et al.’s (2005) study of 4U 0142+61 is the ratio of the optical to X-ray pulsed fraction: in 1E 1048.1–5937 it is approximately unity, whereas in 4U 0142+61 the optical pulsations had an rms pulsed fraction 5–7 times that of the X-rays. However, whereas the optical and X-ray pulsed fractions for 1E 1048.1–5937 were measured contemporaneously, those of 4U 0142+61 were not. The X-ray pulsed fractions of 4U 0142+61 reported by Dhillon et al. (2005) were quoted from the work of Patel et al. (2003), who obtained their *Chandra* data in 2000, over two years prior to the optical observations. We now know from the work of Dib et al. (2007), however, that 4U 0142+61 exhibited an increase in its pulsed light of 36% in the 2–10 keV band between 2002 and 2004. Hence it is possible that at least part of the discrepancy between the optical/X-ray pulsed fraction ratio in 1E 1048.1–5937 and 4U 0142+61 is due to variability in the latter source. This hypothesis is further supported by the fact that Dhillon et al. (2005) measured a value of $h_{pt} = 58 \pm 16\%$ in September 2002 whereas Kern & Martin (2002) measured $h_{pt} = 27 \pm 8\%$ in November 2001, although there are other possible reasons for this discrepancy (see Dhillon et al. 2005 for a discussion). It is also possible that the discrepancy between the optical/X-ray pulsed fraction ratio in 1E 1048.1–5937 and 4U 0142+61 is due to variability in 1E 1048.1–5937: as discussed in section 3.2.1, the X-ray pulsed fraction of 1E 1048.1–5937 is inversely proportional to the total 2–10 keV flux. The optical pulsed fraction might not vary in the same way, implying that the optical/X-ray pulsed fraction ratio in 1E 1048.1–5937 could be variable and we just happened to observe it when it was unity.

Viewed in isolation, the data on 1E 1048.1–5937 presented in this paper do not allow us to discriminate between the magnetar and fallback disc models, as the optical and X-ray pulsed fractions are approximately equal, although the tentative evidence we present for the optical pulses leading the X-rays is irreconcilable with reprocessing. Arguably the most important result of this paper, however, is that it confirms the existence of pulsed optical light in a second AXP, 1E 1048.1–5937, thereby demonstrating that the properties of the optical emission in 4U 0142+61 are not unique. The observed similarities between the optical and X-ray emission in both 1E 1048.1–5937 and 4U 0142+61 indicate that closely related populations of particles, located in the same region of the magnetosphere, are probably responsible for the emission. This paper has also highlighted the way forward for time-resolved optical studies of these incredibly faint objects, as the data presented in this paper would have been unobtainable had 1E 1048.1–5937 been in a faint state. By targetting observations during bright X-ray states, it should be possible to study other AXPs, and possibly also soft gamma repeaters, in the optical part of the spectrum, although this will still require access to sensitive, high-speed cameras like ULTRACAM on the world’s largest telescopes.

ACKNOWLEDGMENTS

ULTRACAM is supported by STFC grant PP/D002370/1. SPL acknowledges the support of an RCUK Fellowship and

STFC grant PP/E001777/1. TRM and CC are supported under STFC grant ST/F002599/1. VMK holds the Lorne Trottier Chair in Astrophysics and Cosmology, a Canada Research Chair and acknowledges support from an NSERC Discovery Grant, CIFAR and FQRNT. RPM acknowledges STFC for support through its rolling grant programme. Based on observations collected at ESO, Chile.

REFERENCES

- Alpar M. A., 2001, *ApJ*, 554, 1245
 Beloborodov A. M., Thompson C., 2007, *ApJ*, 657, 967
 Chatterjee P., Hernquist L., Narayan R., 2000, *ApJ*, 534, 373
 Dhillon V. S., Marsh T. R., Hulleman F., van Kerkwijk M. H., Shearer A., Littlefair S. P., Gavriil F. P., Kaspi V. M., 2005, *MNRAS*, 363, 609
 Dhillon V. S., Marsh T. R., Stevenson M. J., Atkinson D. C., Kerry P., Peacocke P. T., Vick A. J. A., Beard S. M., Ives D. J., Lunney D. W., McLay S. A., Tierney C. J., Kelly J., Littlefair S. P., Nicholson R., Pashley R., Harlaftis E. T., O’Brien K., 2007, *MNRAS*, 378, 825
 Dib R., Kaspi V. M., Gavriil F. P., 2007, *ApJ*, 666, 1152
 Dib et al. R., 2008, in preparation
 Durant M., van Kerkwijk M. H., 2005, *ApJ*, 627, 376
 Durant M., van Kerkwijk M. H., 2006, *ApJ*, 650, 1082
 Ertan Ü., Erkut M. H., Ekşi K. Y., Alpar M. A., 2007, *ApJ*, 657, 441
 Gavriil F. P., Kaspi V. M., 2004, *ApJ*, 609, L67
 Hulleman F., van Kerkwijk M. H., Kulkarni S. R., 2000, *Nat*, 408, 689
 Hulleman F., van Kerkwijk M. H., Kulkarni S. R., 2004, *A&A*, 416, 1037
 Kaspi V. M., Gavriil F. P., Chakrabarty D., Lackey J. R., Muno M. P., 2001, *ApJ*, 558, 253
 Kern B., Martin C., 2002, *Nat*, 417, 527
 Mereghetti S., 2008, *A&AR*, 15, 287
 Naylor T., 1998, *MNRAS*, 296, 339
 Patel S. K., Kouveliotou C., Woods P. M., Tennant A. F., Weisskopf M. C., Finger M. H., Wilson C. A., Göğüş E., van der Klis M., Belloni T., 2003, *ApJ*, 587, 367
 Perna R., Hernquist L., Narayan R., 2000, *ApJ*, 541, 344
 Press W. H., Rybicki G. B., 1989, *ApJ*, 338, 277
 Smith J. A., Tucker D. L., Kent S., Richmond M. W., Fukugita M., Ichikawa T., Ichikawa S., Jorgensen A. M., Uomoto A., Gunn J. E., Hamabe M., Watanabe M., Tolea A., Henden A., Annis J., Pier J. R., McKay T. A., Brinkmann J., Chen B., Holtzman J., Shimasaku K., York D. G., 2002, *AJ*, 123, 2121
 Tam C. R., Gavriil F. P., Dib R., Kaspi V. M., Woods P. M., Bassa C., 2008, *ApJ*, 677, 514
 van Paradijs J., Taam R. E., van den Heuvel E. P. J., 1995, *A&A*, 299, L41
 Wang Z., Bassa C., Kaspi V. M., Bryant J. J., Morrell N., 2008, *ApJ*, 679, 1443
 Woods P. M., Thompson C., 2006, in Lewin W. H. G., van der Klis M., eds, *Compact Stellar X-ray Sources*. CUP, Cambridge, p. 547